J. Fluid Mech. (1984), *vol.* 139, *pp.* 1–28
Printed in Great Britain

The boundary layer induced by a convected two-dimensional vortex

By T. L. DOLIGALSKI

Department of Aerospace and Mechanical Engineering, University of Notre Dame, Notre Dame, Indiana

AND J. D. A. WALKER

Department of Mechanical Engineering and Mechanics, Lehigh University, Bethlehem, Pennsylvania

(Received 5 July 1982 and in revised form 19 July 1983)

The response of a wall boundary layer to the motion of a convected vortex is investigated. The principal cases considered are for a rectilinear filament of strength $-\kappa$ located a distance a above a plane wall and convected to the right in a uniform flow of speed U_∞^*. The inviscid solution predicts that such a vortex will remain at constant height a above the wall and be convected with constant speed αU_∞^*. Here α is termed the fractional convection rate of the vortex, and cases in the parameter range $0 \leqslant \alpha < 1$ are considered. The motion is initiated at time $t^* = 0$ and numerical calculations of the developing boundary-layer flow are carried out for $\alpha = 0, 0.2, 0.4, 0.55, 0.7, 0.75$ and 0.8. For $\alpha < 0.75$, a rapid lift-up of the boundary-layer streamlines and strong boundary-layer growth occurs in the region behind the vortex; in addition an unusual separation phenomenon is observed for $\alpha \leqslant 0.55$. For $\alpha \geqslant 0.75$, the boundary-layer development is more gradual, but ultimately substantial localized boundary-layer growth also occurs. In all cases, it is argued that a strong inviscid–viscous interaction will take place in the form of an eruption of the boundary-layer flow. The generalization of these results to two-dimensional vortices with cores of finite dimension is discussed.

1. Introduction

Effectively inviscid flows containing vorticity occur in a wide variety of fluid motions of familiar experience. However, relatively little is known about how such flows interact with the viscous boundary layers which must be present on all solid walls in any real fluid. One such interaction ocurs in the flow over the upper surface of a slender delta wing at angle of attack (Harvey 1958; Ornberg 1964); here the vortex sheet shed from the leading edge of the wing is rolled up into a vortex above the upper surface of the wing. The convected vortex was subsequently observed to interact with the boundary-layer flow in the vicinity of the wing surface to induce a secondary separation in the form of a recirculating eddy near the wing surface. A second example of an interaction is observed between the trailing vortices produced at the tip of an aircraft wing and the boundary layer formed on the ground. This type of flow has been simulated experimentally by Harvey & Perry (1971), who mounted a single wing in the test section of a wind tunnel; in order to simulate conditions on a take-off or landing, the test section had a moving belt on the floor. The trailing vortex created at the wing tip convected outboard over the moving belt

and was observed to induce a boundary-layer separation in the vicinity of the moving belt in the form of a secondary vortex. Ultimately the spawned vortex was ejected from the wall region, slowing the horizontal motion of the parent vortex and causing it to rise. The secondary vortex is created in an unsteady separation and subsequent interaction phenomenon which initiates in the boundary layer; the problem has been investigated theoretically by Walker (1978), who obtains close agreement with the measured results of Harvey & Perry. Note that the phenomenon is unusual and difficult to observe since it develops and takes place in a frame of reference convecting with the parent vortex; consequently, although a number of investigators had noted a 'rebounding' effect of aircraft vortices as they approached the ground plane, the reasons for the phenomenon are only apparent upon close examination of the nature of the boundary-layer flow. This particular example is important since there is incontrovertible experimental (Harvey & Perry 1971) and theoretical (Walker 1978) evidence to show how a parent vortex can induce a boundary-layer separation leading to the formation of a secondary vortex.

In both of the cited examples, a region of *concentrated* vorticity in an otherwise irrotational flow induces an inviscid–viscous interaction in the form of a boundary-layer eruption. Situations where the vorticity is *continuously* distributed in an inviscid flow also occur frequently; for example in turbo-machinery, the wake shed from each blade row is rotational and can be expected to interact with the boundary layers on succeeding blades. A popular technique used to simulate flows having a continuous distribution of vorticity is the discrete vortex method summarized by Clements & Maull (1975). In this method, a continuous vorticity distribution is represented by a collection of discrete vortices whose positions at any time are computed using an initial-value integration method; the main motivation of this approach is a hope that the flow field under study may be modelled by a reasonably small number of vortices and thus the massive computer storage requirements associated with numerical solutions of the Navier–Stokes equation may be avoided. Various authors have adopted this approach to investigate the shear layers formed on solid surfaces in a viscous fluid (see e.g. Clements & Maull 1975). Normally in such studies, vortices are periodically introduced into the flow field at flow separation points; such points may be readily apparent from the geometry of the problem (e.g. downstream corners) or may have to be determined from empirically motivated correlations. In these approaches, image vortices are produced within the wall or body under study in order to produce a vanishing inviscid velocity normal to all solid surfaces; however, the no-slip condition for the tangential velocity is not satisfied at solid walls, and consequently it is tacitly assumed that the boundary layers remain thin and passive for all time. It is therefore of interest to determine the effect of convected rotational disturbances on a boundary-layer flow.

Another motivation for the present study is associated with turbulent boundary layers. Three-dimensional vortex structures are known to be an important feature of turbulent boundary-layer flows (Willmarth 1975; Falco 1977, 1978; Nychas, Hershey & Brodkey 1973). The turbulent boundary layer is a composite double layer consisting of a relatively thick outer layer and a thin inner wall layer. Convected vorticular structures are readily observed in the outer sublayer of the boundary layer; on the other hand the wall layer is observed to be in a passive or quiescent state for the majority of a particular observation time. This quiescent wall-layer state is observed to be cyclically interrupted with an explosive eruption of wall-layer fluid into the outer layer in an event usually referred to as the bursting phenomenon. The bursting process is the mechanism by which a turbulent boundary layer maintains

itself, as new vorticity is continually generated and ejected from the wall region in a strong inviscid–viscous interaction with the outer-layer flow. Although Nychas *et al.* (1973) reported that ejections of wall-layer fluid appeared to be associated in some way with the passage of vorticular motions in the outer layer, the causes of the bursting event are not yet well understood.

In this study, the effects of convected rotational disturbances on boundary layers will be explored in what perhaps is the most fundamental context (a more complex case corresponding to a vortex in a shear flow is discussed by Doligalski, Smith & Walker 1980; Doligalski 1980). In particular, the case of a rectilinear vortex convected in a uniform flow above a plane wall will be investigated. The motion is assumed to be initiated at time $t^* = 0$, and, for all $t^* > 0$, a thin boundary layer will develop and grow on the plane wall. The object of this paper is to investigate the expected terminal behaviour of the boundary layer for various convection rates of the vortex relative to uniform flow. Specifically, it is of interest to examine whether the boundary layer will remain thin or whether a boundary-layer breakdown may be expected at some stage. Here, following Riley (1975), the term breakdown is understood to imply a catastrophe with respect to the boundary-layer equations in which 'the notion of a thin boundary layer embedded in an otherwise inviscid flow fails'. Such a breakdown culminates physically in a viscous–inviscid interaction between the boundary layer and the outer inviscid flow, and can, in general, be expected to modify the inviscid flow substantially.

In the present study, the vortex has strength $-\kappa$, is located a distance a above the wall and is convected with speed αU_∞^* in a uniform flow of speed U_∞^*. The fractional convection rate α is decreased by decreasing a or by increasing κ, and values of α in the range $[0,1]$ are of interest here. The plan of the paper is as follows. In §2 the relevant features of the inviscid flow are discussed; in §3 the boundary-layer problem is formulated and the numerical solution procedure is described in §4. In §5 calculated results for $\alpha = 0$ are discussed. In §6 the case of a convected vortex is addressed and results are presented for $\alpha = 0.2$, 0.4, 0.55, 0.7, 0.75 and 0.8. In all cases, strong boundary-layer growth was observed in the region behind the vortex and considerable difficulty was encountered in advancing the numerical solutions beyond a certain point in time despite the development of a new numerical scheme. In §7 it is argued that an inviscid–viscous interaction will occur for all convection rates. The precise nature of the interaction is not known since it has not proved possible to determine the analytical structure of the terminal form of the boundary-layer solution (immediately preceding interaction). In any case, it is suggested that the expected interaction will culminate in the creation of a secondary vortex. In addition it is argued that the present results for the rectilinear filament may be representative of discrete vortex motion in two dimensions.

2. The inviscid flow

Consider first the inviscid flow due to a rectilinear vortex of negative rotation $-\kappa$ located a distance a from an infinite plane wall at $y^* = 0$. The inviscid solution (Milne-Thomson 1962, p. 359) predicts that the vortex will convect to the left at constant speed $V_c = \kappa/2a$ and remain at constant height $y^* = a$ as it moves under the influence of the image vortex (of positive rotation $+\kappa$) at $y^* = -a$. If a uniform flow of speed U_∞^* is superimposed to the right, the vortex convects to the right with speed

$$V_c = U_\infty^* - \kappa/2a. \tag{1}$$

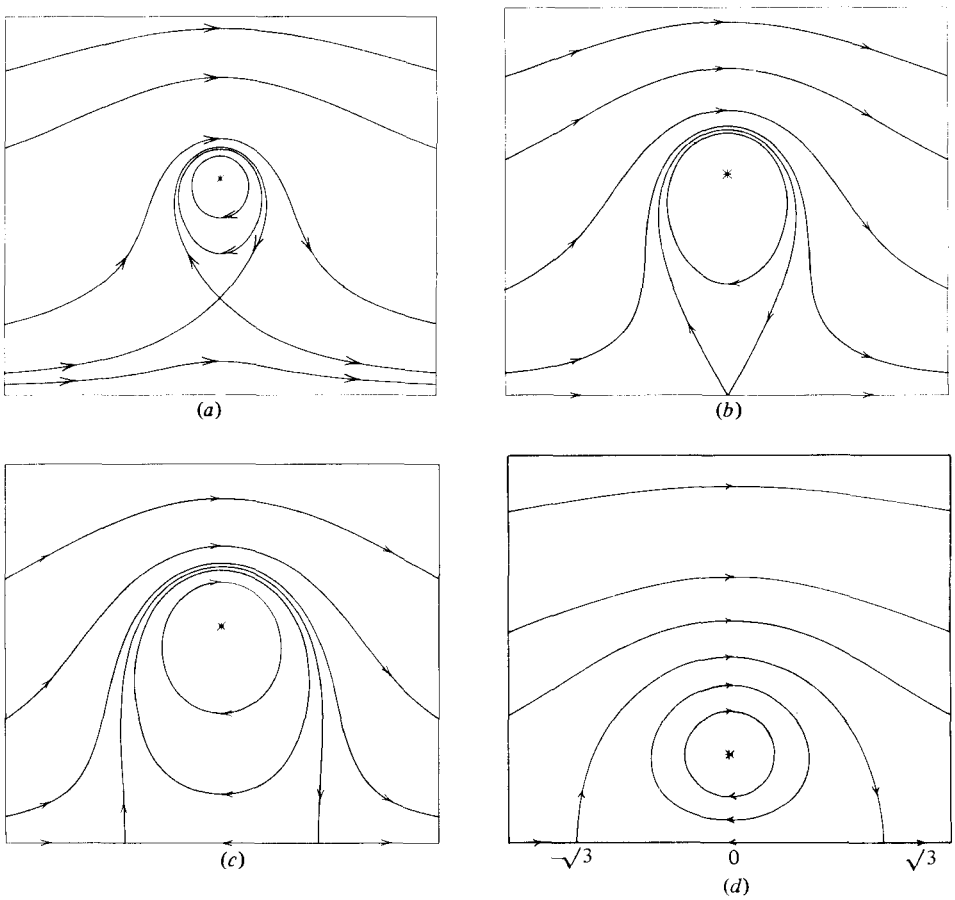

FIGURE 1. Instantaneous streamlines in the laboratory frame for the inviscid flow for (*a*) $\alpha = 0.80$, (*b*) $\alpha = 0.75$, (*c*) $\alpha = 0.70$, (*d*) $\alpha = 0$. Also, (*d*) represents the streamline patterns for all α in a frame of reference convecting with the vortex; the scale of (*d*) is 2.5 times larger than in (*a*)–(*c*).

Define a fractional convection rate α as the ratio of the self-induced vortex speed to the uniform flow speed, according to

$$\alpha = \frac{V_c}{U_\infty^*} = 1 - \frac{\kappa}{2aU_\infty^*}. \tag{2}$$

In this study the parameter range $0 \leqslant \alpha < 1$ is of interest. For a mixed uniform flow speed U_∞^*, the fractional convection rate α decreases as the vortex is moved closer to the wall or as the absolute strength of the vortex is increased. The lower limit $\alpha = 0$ corresponds to a vortex which is either strong enough or close enough to the wall so that the self-induced velocity exactly balances the uniform flow speed and the vortex is held stationary in a crossflow. In the upper limit as $\alpha \to 1$, either $\kappa \to 0$ and there is no vortex or the distance from the wall and/or the uniform flow speed becomes large; in either situation the inviscid flow near $y^* = 0$ is essentially a uniform flow.

It is worthwhile to consider briefly the physical significance of other values of α, although such cases will not be treated explicitly in this study. For $\alpha < 0$, the vortex above the wall $y^* = 0$ is either strong enough or close enough to the wall so that it propagates in the negative x^* direction upstream against the uniform flow. For $\alpha > 1$

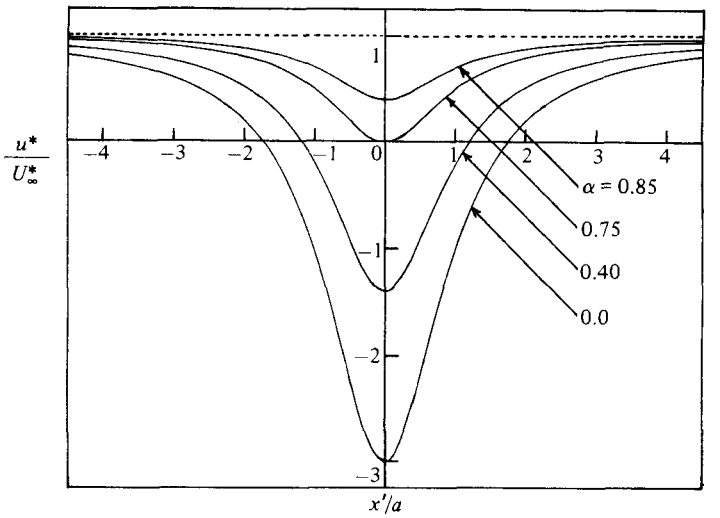

FIGURE 2. Instantaneous inviscid velocity distribution near the wall in the laboratory frame for various values of the relative convection speed of the vortex.

the assumed sense of the rotation of the vortex is reversed and becomes positive; in this case the vortex moves to the right with speed $V_c > U_\infty^*$; the case $\alpha \to \infty$ corresponds to the case previously investigated by Walker (1978).

The complex potential describing the inviscid flow at any time t^* is easily obtained (Milne-Thomson 1962), with the result

$$\omega = U_\infty^* z + \mathrm{i}\kappa \log\left\{\frac{z - \mathrm{i}a - \alpha U_\infty^* t^*}{z + \mathrm{i}a - \alpha U_\infty^* t^*}\right\}, \tag{3}$$

where z is the complex variable $x^* + \mathrm{i}y^*$;† here x^* measures distance in the streamwise direction, and the vortex is assumed to be located at $x^* = 0$, $y^* = a$ at $t^* = 0$. It is of interest to examine the nature of the inviscid flow, and in figures 1 (a, b, c) the instantaneous flow patterns are plotted for $\alpha = 0.8$, 0.75, 0.7 respectively. These figures are all drawn to the same scale and correspond to the instantaneous flow patterns that an observer in the laboratory frame would see at a fixed value of t^*. In general for $\alpha > 0.75$ (figure 1a) a stagnation point occurs above the wall, and this point approaches the wall as α decreases to a critical value of $\alpha = 0.75$ (figure 1b). As α decreases below the critical value (figure 1c), two stagnation points occur near the wall; for decreasing α these points move progressively outboard of the vortex centre, and eventually as $\alpha \to 0$ approach the limiting values of $x' = \pm\sqrt{3}a$, where $x' = x^* - V_c t^*$, as depicted in figure 1(d). Note that the scale of figure 1(d) is 2.5 times larger than any of figures 1$(a$–$c)$; the axes in these figures are x'/a and y^*/a, and the asterisk denotes the vortex centre.

The unsteady inviscid velocity near the wall may be evaluated from (3) (Milne-Thomson 1962) and as $y^* \to 0$ the velocity components are such that

$$\frac{u^*}{U_\infty^*} = 1 - \frac{4a^2(1-\alpha)}{x'^2 + a^2}, \quad v^* \to 0. \tag{4a,b}$$

The streamwise velocity given by $(4a)$ is plotted for various values of α in figure 2. For $\alpha < 0.75$, the effects of the vortex are strong enough so that a reversed-flow region

† The definition of ω used here differs from that of Milne-Thomson by a minus sign.

bounded by two stagnation points is observed in the laboratory frame near the wall in the region immediately below the vortex. In all cases the point of minimum velocity occurs immediately below the vortex and an absolute minimum of $-3U_\infty^*$ occurs at $\alpha = 0$. For $\alpha = 0.75$ the two stagnation points coincide at a point directly below the moving vortex and no reversed flow occurs near the wall. For $\alpha > 0.75$, the flow near the wall is retarded under the vortex but is always in the positive x^* direction.

In a frame of reference which convects uniformly with the vortex the inviscid flow is steady and the wall moves to the left with velocity $-\alpha U_\infty^*$. The complex potential in the convected frame is easily obtained from (3) by superimposing a uniform flow equal and opposite to that of the vortex. It is readily verified that for all values of α the inviscid flow relative to the vortex is identical to that depicted in figure 1(*d*). In the convected reference frame, the curve labelled $\alpha = 0$ in figure 2 describes the normalized tangential velocity $u^*/\{(1-\alpha)\,U_\infty^*\}$ near the wall for all α. It may be observed that there is a deceleration in the inviscid flow near the wall, from upstream infinity toward what will be termed the front stagnation point; this stagnation point is characterized by flow toward the wall. Behind the front stagnation point a strong reverse acceleration occurs to an absolute minimum of -3 immediately underneath the vortex at $x^* = 0$. Behind the vortex centre, the magnitude of the velocity decreases monotonically to zero toward the rear stagnation point; this stagnation point is characterized by flow away from the wall. Beyond the rear stagnation point a slow acceleration occurs toward downstream infinity.

The inviscid solution is not uniformly valid and a boundary layer is required to satisfy the no-slip condition at the wall; this problem is formulated in §3.

3. The boundary-layer problem

In the present study, the principal interest is in the terminal nature of the boundary-layer flow induced by a convected vortex and to consider the evolution of the boundary layer it is necessary to specify an initial condition. Here the simplest initial state is considered wherein the wall suddenly enters the flow at $t^* = 0$; alternatively it may be imagined that the effects of viscosity become important abruptly at $t^* = 0$. This impulsive start initial condition is virtually impossible to reproduce experimentally; however, the main purpose of this study is to determine whether or not the boundary layer responds to the discrete vorticity present in the inviscid flow in such a way that a local breakdown of the boundary-layer flow is to be expected. The numerical solutions to be described here suggest that breakdown will occur for all values of α; consequently the selected initial condition is not considered important for demonstrating the basic effect and should be regarded only as a convenient mathematical state from which the boundary-layer development may be computed forward in time.

Choosing a Cartesian coordinate system (x^*, y^*) with corresponding velocity components (u^*, v^*) which convects uniformly with the vortex, the following dimensionless boundary-layer variables are defined:

$$\left.\begin{aligned} x = \frac{x^*}{a}, \quad y = \frac{y^*}{a} Re^{\frac{1}{2}}, \quad t = U_\infty^*(1-\alpha)\frac{t^*}{a}, \\ u = \frac{u^*}{U_\infty^*(\alpha-\alpha)} \quad v = \frac{v^*}{U_\infty^*(1-\alpha)} Re^{\frac{1}{2}}, \end{aligned}\right\} \tag{5}$$

where the Reynolds number is defined as $Re = (1-\alpha)\, U_\infty^* a/\nu$, with ν being the kinematic viscosity. The reference velocity $(1-\alpha)\, U_\infty^*$ in these definitions corresponds to the inviscid velocity near the wall far upstream of the vortex as seen by an observer in the convected frame. The incompressible equations governing the unsteady laminar boundary-layer flow are

$$\frac{\partial u}{\partial t}+u\frac{\partial u}{\partial x}+v\frac{\partial u}{\partial y}=U_\infty\frac{\mathrm{d}U_\infty}{\mathrm{d}x}+\frac{\partial^2 u}{\partial y^2}, \quad \frac{\partial u}{\partial x}+\frac{\partial v}{\partial y}=0, \tag{6}$$

where the mainstream velocity is

$$U_\infty = 1-\frac{4}{x^2+1}. \tag{7}$$

The boundary conditions associated with (6) are

$$\left.\begin{aligned} &u=-\beta, \quad v=0 \quad \text{at} \quad y=0,\\ &u\to U_\infty(x) \quad \text{as} \quad y\to\infty, \end{aligned}\right\} \tag{8}$$

where

$$\beta=\frac{\alpha}{1-\alpha}. \tag{9}$$

Here the parameter β represents the ratio of the vortex convection velocity V_c to the inviscid velocity near the wall at upstream infinity in the moving reference frame. The initial condition corresponds to abruptly imposing the no-slip condition $u=-\beta$ at $t=0$. The boundary-layer problem is inherently unsteady, since the flow at upstream and downstream infinity corresponds to a classical Rayleigh (1911) problem in which the boundary layer continuously thickens proportionally to $t^{\frac{1}{2}}$. The object here is to determine whether other phenomena take place in the boundary layer near the vortex which lead to much more dramatic boundary-layer growth.

It is convenient to introduce a new streamwise coordinate defined by the Görtler-type transformation

$$\xi=\frac{1}{2\pi}\int_x^\infty \frac{4\,\mathrm{d}x}{1+x^2}=1-\frac{2}{\pi}\arctan x. \tag{10}$$

This transformation is one-to-one and transforms the x-interval $(-\infty,\infty)$ to the finite range $[2,0]$ respectively. In the ξ-coordinate the front and rear stagnation points are at $\xi=\frac{1}{3}$ and $\frac{5}{3}$ respectively, and the location of the vortex centre is at $\xi=1$. The mainstream velocity in (7) becomes

$$U_\infty = 1-U_e(\xi), \quad U_e(\xi)=2(1-\cos\pi\xi). \tag{11}$$

An unsteady stream function $\psi(\xi,y,t)$ is introduced according to

$$u=\frac{\partial\psi}{\partial y}, \quad v=\frac{1}{2\pi}U_e(\xi)\frac{\partial\psi}{\partial\xi}, \tag{12}$$

which identically satisfies the continuity equation. The boundary layer initially has a thickness proportional to $t^{\frac{1}{2}}$, and it is convenient to introduce Rayleigh variables (Blasius 1908; Rayleigh 1911) according to

$$\eta=\frac{y}{2t^{\frac{1}{2}}}, \quad \psi=2t^{\frac{1}{2}}\Psi(\xi,\eta,t). \tag{13}$$

The boundary-layer equations (6) become

$$\frac{\partial^3 \Psi}{\partial \eta^3} + 2\eta \frac{\partial^2 \Psi}{\partial \eta^2} - 4t \frac{\partial^2 \Psi}{\partial \eta \, \partial t} = \frac{2U_e(\xi)}{\pi} t \left\{ -2\pi \sin \pi\xi (2\cos \pi\xi - 1) - \frac{\partial \Psi}{\partial \eta} \frac{\partial^2 \Psi}{\partial \xi \, \partial \eta} + \frac{\partial \Psi}{\partial \xi} \frac{\partial^2 \Psi}{\partial \eta^2} \right\} \tag{14}$$

and the associated boundary conditions are

$$\Psi(\xi, 0, t) = 0, \quad \frac{\partial \Psi}{\partial \eta}(\xi, 0, t) = -\beta, \tag{15}$$

$$\frac{\partial \Psi}{\partial \eta} \to 2\cos \pi\xi - 1 \quad \text{as} \quad \eta \to \infty. \tag{16}$$

At upstream and downstream infinity (corresponding to $\xi = 0$ and 2 respectively) $U_e(\xi) = 2(1 - \cos \pi\xi) \to 0$ and the right-hand side of (14) vanishes; here the boundary-layer problem reduces to a Rayleigh-type flow wherein the boundary layer must adjust a unit mainstream velocity to $-\beta$ on the wall. The solution to this problem is readily obtained, and is

$$\frac{\partial \Psi}{\partial \eta} = U_R(\eta) = -\beta + (1 + \beta) \operatorname{erf} \eta. \tag{17}$$

This is a vortex-sheet flow which provides a smooth transition in the boundary layer between the left-moving plate and the right-moving uniform flow. The solution for $0 < \xi < 2$ is to be advanced forward in time numerically; at any fixed time, the numerical solution in the (ξ, η)-plane is computed iteratively in a manner similar to those associated with boundary-value problems. The solution (17) provides the boundary conditions for all t at $\xi = 0, 2$.

The initial conditions for (14), corresponding to the abrupt insertion of the plate in the flow, are obtained using a well-known procedure (Blasius 1908; Walker 1978) in which Ψ is expanded in a power series in time according to

$$\Psi = \Psi_0(\xi, \eta) + t\Psi_1(\xi, \eta) + \ldots. \tag{18}$$

Upon substitution in (14), a sequence of problems for each function in (18) may be obtained. The first term in (18) is

$$\frac{\partial \Psi_0}{\partial \eta} = -\beta + (\beta - 1 + 2\cos \pi\xi) \operatorname{erf} \eta, \tag{19}$$

which provides the initial boundary-layer solution for all ξ at $t = 0^+$. The second term in (18) is of the form

$$\frac{\partial \Psi_1}{\partial \eta} = U_e(\xi) \sin \pi\xi \{g'_{12}(\eta) + \beta g'_{11}(\eta)\}, \tag{20}$$

where the functional coefficients g'_{12} and g'_{11} are given explicitly by Doligalski (1980). In principle it is possible to calculate further terms in (18), but the process becomes rather tedious and in any case the solution procedure is restricted to small times. To extend the solution to larger times it is necessary to calculate the solution of (14) numerically, and the finite-difference method is considered next.

4. The numerical solution

In the computational method, it is convenient to write the velocity as a linear combination of the Rayleigh flow at infinity plus a term due to the disturbing vortex motion according to

$$\frac{\partial \Psi}{\partial \eta} = U_{\mathrm{R}}(\eta) - U_{\mathrm{e}}(\xi)\, U(\xi, \eta), \tag{21}$$

where U_{R} is given by (17). The boundary conditions for the velocity disturbance U follow from (15) and (16), and are

$$U(\xi, 0) = 0, \quad U(\xi, \eta) \to 1 \quad \text{as} \quad \eta \to \infty. \tag{22}$$

The main motivation for this transformation is that U varies from 0 at the wall to 1 at the boundary-layer edge for all ξ; thus U may be interpreted as a normalized velocity which is convenient for computational purposes, particularly for monitoring boundary-layer growth as the calculation proceeds. Under the transformation (21), (14) becomes

$$4t\frac{\partial U}{\partial t} = \frac{\partial^2 U}{\partial \eta^2} + P\frac{\partial U}{\partial \eta} + RU + Q\frac{\partial U}{\partial \xi} + S, \tag{23}$$

where

$$\left.\begin{aligned} P &= 2\eta + \frac{2t}{\pi} U_{\mathrm{e}}\left[U'_{\mathrm{e}} f + U_{\mathrm{e}} \frac{\partial f}{\partial \xi} \right], \\ Q &= \frac{2t}{\pi} U_{\mathrm{e}}\left[U_{\mathrm{R}}(\eta) - U_{\mathrm{e}}(\xi)\, U \right], \\ R &= \frac{2t}{\pi} U'_{\mathrm{e}}\left[U\mathrm{R}(\eta) - U_{\mathrm{e}}(\xi)\, U \right], \\ S &= -\frac{2t}{\pi}\left[U'_{\mathrm{e}}(1 - U_{\mathrm{e}}) + U'_{\mathrm{R}}\left(U'_{\mathrm{e}} f + U_{\mathrm{e}} \frac{\partial f}{\partial \xi} \right) \right]. \end{aligned}\right\} \tag{24}$$

Here

$$\frac{\partial f}{\partial \eta} = U, \quad U_{\mathrm{e}}(\xi) = 2(1 - \cos \pi\xi), \tag{25a, b}$$

and f may be termed a vortex-disturbance stream function.

A rectangular grid in the (ξ, η)-plane was defined with uniform mesh sizes in the ξ- and η-directions denoted by h_1 and h_2 respectively; in all cases h_1 was selected so that mesh lines were at $\xi = \frac{1}{3}$ and $\xi = \frac{5}{3}$, which correspond to the streamwise locations of the front and rear stagnation points respectively. The second of the conditions (22) must be imposed at some large but finite value of η, say $\eta = l$, as an approximation, and l must be increased until there is no significant change in the solution at any value of t. Throughout the early stages of the integrations a value of $l = 6$ was found to be adequate for all values of β. However, substantial boundary-layer growth eventually occurred for all cases in the vicinity of the rear stagnation point, and it was necessary to increase l to 8 and in some cases larger values in the latter stages of the integrations.

A number of different mesh sizes and time steps were used as a check on the accuracy, and agreement between successive solutions was excellent. In the initial phases of the motion, variations with time are relatively intense, and a small

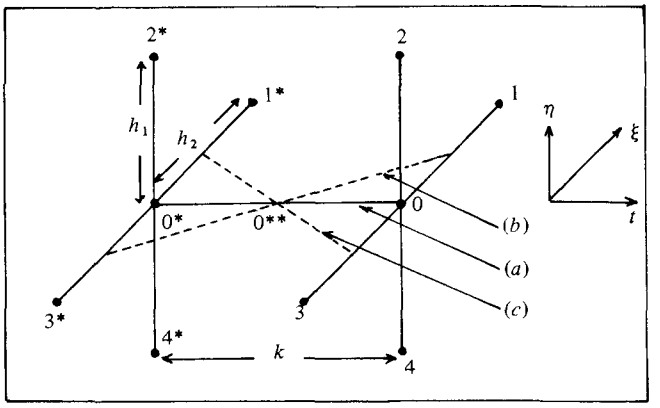

FIGURE 3. Schematic diagram of the grid structure at a typical mesh point 0 in the (ξ, η)-plane; (*a*) denotes averaging path for the Crank–Nicolson method, while (*b*) and (*c*) are the paths for the alternative method.

time step Δt was used. Typically the time step was progressively increased from $\Delta t = 0.001$ near $t = 0$ to $\Delta t = 0.025$ for $t > 0.025$ and then held constant for the balance of the integrations. Two sets of mesh sizes for (h_1, h_2) were used, corresponding to (0.0167, 0.1) and (0.0111, 0.0667).

Two numerical finite-difference schemes were used to solve (23), and these will now be described. In figure 3 the Southwell notation is used to denote a typical mesh point in the (ξ, η)-plane at time t by 0, with the surrounding points labelled 1, 2, 3 and 4; corresponding points in the previous time plane are denoted similarly but with an asterisk. In both numerical methods the partial differential equation (23) is approximated at the point labelled 0** in figure 3 which is midway between the points 0 and 0* on the line labelled (*a*). If the right-hand side of (23) is denoted by D, the Crank–Nicolson approximation to (23) is

$$\frac{4}{\Delta t}\left\{t-\frac{\Delta t}{2}\right\}(U_0 - U_0^*) = \tfrac{1}{2}(D_0 + D_0^*), \tag{26}$$

where the truncation error is $O(\Delta t^2)$, with Δt being the time step. The right-hand side of (26) contains first and second derivatives with respect to ξ and η, which, in the usual Crank–Nicolson method (Walker 1978), are approximated with second-order central-difference formulae in the current and previous time planes. Consequently the overall accuracy of the method is second-order accurate in both space directions and time. These difference approximations lead to a difference equation at each internal mesh point, and the large set of difference equations is solved using iterative methods. Because the difference equations are nonlinear, linearization is necessary at any stage in the iteration procedure. The difficulty that may be encountered, particularly when the flow field begins to develop intense variations locally, is that the matrix problem associated with the iteration procedure may fail to be diagonally dominant as a consequence of the central-difference spatial approximations. In such cases, divergence of the iteration procedure usually occurs. In the present study, substantial difficulties were encountered in the latter stages of the integrations as intense variations ultimately develop in the boundary layer behind the vortex centre and the rear stagnation point ($1.67 < \xi < 1.0$). Eventually the numerical scheme based on the usual Crank–Nicolson method failed to converge. This type of difficulty is often experienced with unsteady boundary-layer problems involving separation and substantial boundary-layer growth (see e.g. Belcher *et al.* 1971). To attempt to

overcome the problem and extend the integrations to higher times, an alternate scheme was developed.

The alternate method affects only the evaluation of the terms $P\,\partial U/\partial\eta$ and $Q\,\partial U/\partial\xi$ in (23); the method of differencing is similar to an alogorithm known as 'MacCormack's method' for the computation of time-dependent inviscid supersonic flows (see e.g. MacCormack 1969), and has also been used in conjunction with the Keller-box method by Cebeci (1979), who refers to the approach as the zigzag method. Consider first the term $Q\,\partial U/\partial\xi$ which is approximated at point 0** in figure 3. It can easily be shown that an average, taken along any line passing through 0** and composed of a simple average of the values on the current and previous time planes, is second-order accurate in the time step Δt. In particular, consider the line labelled (*b*) in figure 3 which intersects the lines connecting the mesh points 0 and 1 and 3* and 0* in the previous time plane at the midpoints; once the average is taken along this line, the derivative $\partial U/\partial\xi$ may be approximated with central-difference formulae, and the result is

$$Q\frac{\partial U}{\partial\xi} = \frac{Q_0^{**}}{2}\left\{\frac{U_1 - U_0}{h_1} + \frac{U_1^* - U_3^*}{h_1}\right\}. \tag{27}$$

In (27) the coefficient Q_0^{**} was evaluated during the iterative procedure using a simple average along the line (*a*) in figure 3. When the current value of Q_0^{**} was positive at any stage in the iteration at a particular internal mesh point, (27) was used. On the other hand if $Q_0^{**} < 0$, the difference approximation is based on an average taken along the line labelled (*c*) in figure 3, and this is

$$Q\frac{\partial U}{\partial\xi} = \frac{Q_0^{**}}{2}\left\{\frac{U_0 - U_3}{h_1} + \frac{U_1^* - U_0^*}{h_1}\right\}. \tag{28}$$

The apparent similarity of this method to upwind–downwind differencing should be noted; however, with averaging carried out along the slanted lines (*b*) and (*c*), the difference approximations in (27) and (28) are second-order accurate in both Δt and h_1. For the term $P\,\partial U/\partial\eta$, the approach is similar, giving

$$\left.\begin{aligned} P\frac{\partial U}{\partial\eta} &= \frac{P_0^{**}}{2}\left\{\frac{U_2 - U_0}{h_2} + \frac{U_0^* - U_4^*}{h_2}\right\} \quad (P_0^{**} > 0), \\ &= \frac{P_0^{**}}{2}\left\{\frac{U_0 - U_4}{h_2} + \frac{U_2^* - U_0^*}{h_2}\right\} \quad (P_0^{**} < 0), \end{aligned}\right\} \tag{29}$$

and these approximations are second-order accurate in Δt and h_2. Note that the matrix problem associated with these approximations is always diagonally dominant. To test the alternative method, calculations were carried out in the early stages of the motion using both methods, and the results were virtually identical. However, an important feature of the alternate method is that it allows extension of the numerical integrations to larger times beyond the point where the conventional Crank–Nicolson method failed. In all cases, the method used to integrate (25*a*) was based on a modified Simpson's rule (Dennis & Walker 1971).

5. The stationary vortex

The case of the stationary vortex ($\alpha = 0$) in a crossflow is considered first; here the image-induced velocity acting to the left is exactly balanced by the freestream velocity to the right and the vortex remains stationary at constant height above the plate. In figures 4(*a–d*) the time-dependent development of the streamlines in the

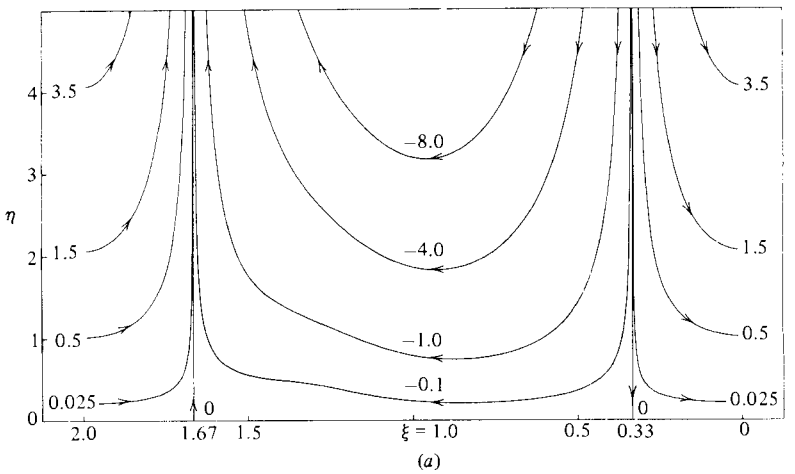

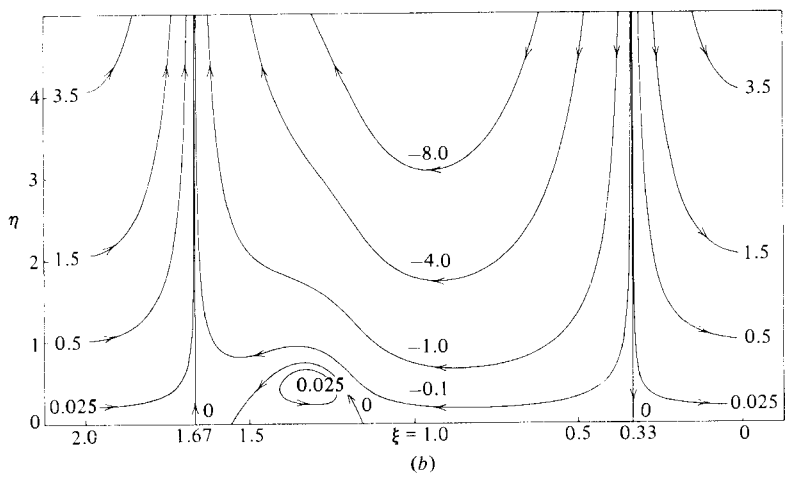

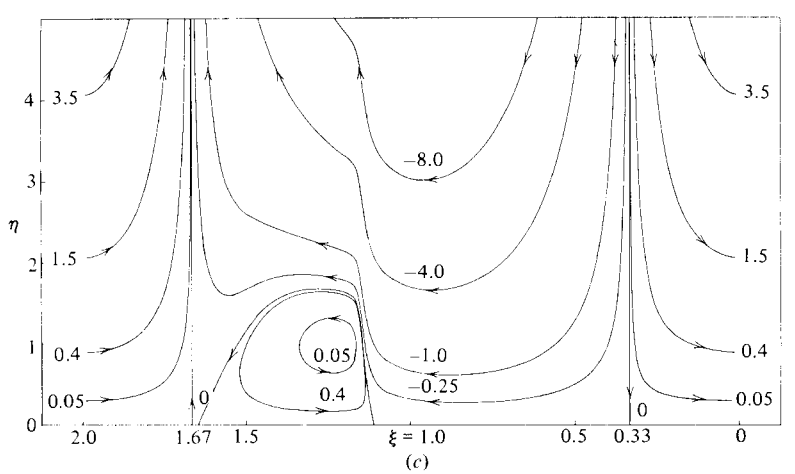

FIGURE 4(*a–c*). For caption see facing page.

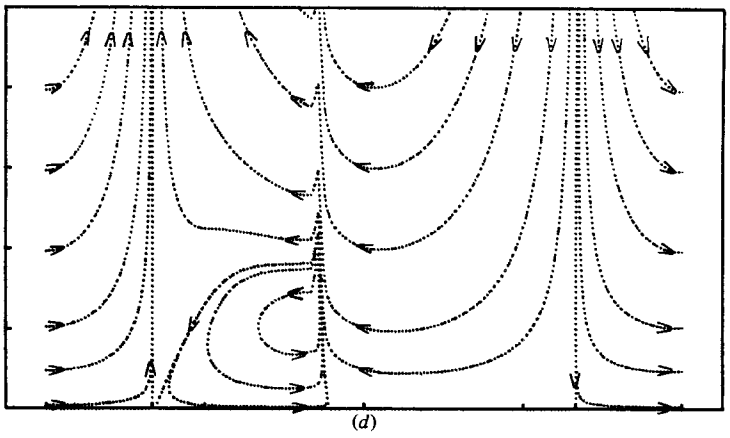

FIGURE 4. Instantaneous streamlines in the boundary layer for the stationary vortex ($\alpha = 0$) at (*a*) $t = 0.2$, (*b*) 0.4, (*c*) 0.65, (*d*) 0.7. (Labels correspond to lines of constant Ψ.)

boundary layer is illustrated. These plots show the instantaneous streamlines in the (ξ, η)-plane, which is convenient to illustrate the flow patterns over the entire range from upstream to downstream infinity. Note, however, that there is a distortion due to the transformation (10) in the flow patterns corresponding to a relative compression of the far-field flow and an exaggeration of the region below the vortex.

The streamlines at $t = 0.2$ are depicted in figure 4(*a*), and it may be observed that the flow patterns in the initial stages are almost symmetrical in the boundary layer about the vortex centre. In this figure and all subsequent streamline plots the labels correspond to constant Ψ-values and the arrows indicate the direction of flow. For $0 < \xi < 0.33$ the motion is downward and toward upstream infinity, while, for $1.67 < \xi < 2$, the flow in the boundary layer is inward from downstream infinity and upward toward the rear stagnation point. Between the stagnation points in the inviscid flow ($0.33 < \xi < 1.67$) the flow patterns are characterized by downflow near the front stagnation point ($\xi = 0.33$) and subsequent upflow near the rear stagnation point ($\xi = 1.67$).

As time passes, the streamlines rapidly begin to lift up in the region behind the vortex and begin to develop a kink; at $t_s = 0.248$ an unsteady separation effect in the form of a closed recirculating eddy of positive rotation attached to the wall was observed to form at $\xi_s = 1.344$. In figure 4(*b*) the flow patterns are illustrated at $t = 0.4$, a short time after the separation has occurred. The subsequent time-dependent development of the eddy is typical of that observed in the classical separation problems which occur behind bluff bodies (see e.g. Dennis & Walker 1972; Collins & Dennis 1973); immediately following the initial appearance of the closed recirculation zone, the eddy grows rapidly in the tangential direction. A period of accelerated and rapid growth in a direction normal to the wall then occurs, and the situation at $t = 0.65$ is illustrated in figure 4(*c*). Shortly after $t = 0.65$ the Crank–Nicolson procedure failed to converge and the calculations could only be carried further in time using the alternate forward–backward scheme; eventually around $t = 0.75$ this scheme failed to converge as well. The reason for the failure of the numerical procedures can be traced to the intense variations which develop in the boundary layer on the right-hand side of the eddy; such variations are evident in figure 4(*c*) and ultimately lead to the behaviour in the numerical solution illustrated in figure 4(*d*) at $t = 0.70$. In figure 4(*d*) it may be observed that the streamlines near the

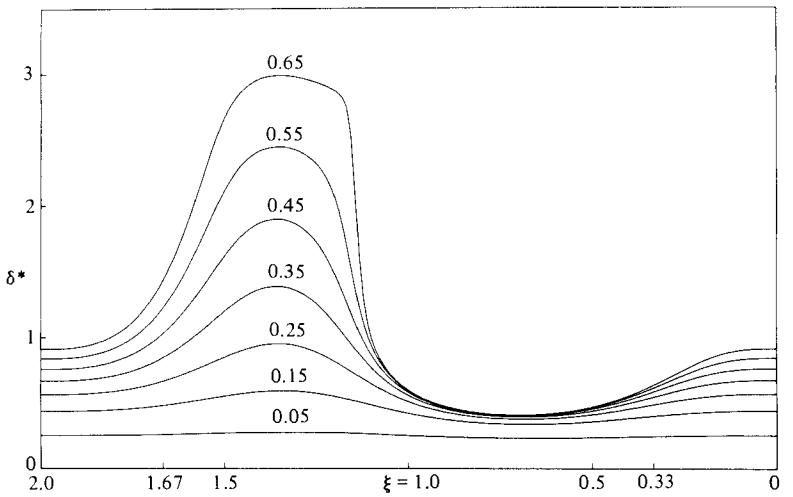

FIGURE 5. Temporal development of displacement thickness for stationary vortex ($\alpha = 0$). (Labels correspond to values of t.)

right-hand side of the eddy have begun to develop a spike-like behaviour; a similar difficulty was encountered by Walker (1978) on the upstream side of a detached separated eddy. The phenomenon illustrated in figure 4(*d*) is suggestive of the early stages of the development of a singular behaviour in the boundary-layer solution. At the stages of the integrations depicted in figures 4(*c*, *d*) the numerical outer boundary was at $l = 8$; from a close examination of the results of the calculations, this value appears adequately large, and the thickening of the boundary layer which occurs in the vicinity of the eddy does not appear to be the major obstacle to continuing the integrations. The main difficulty appears to be associated with the developing intense variations on the right side of the eddy. The calculations were carried out on a CDC 6500; when the integrations were terminated there were approximately 2.2×10^4 points in the mesh, and because of core limitations the mesh could not be further reduced. To illustrate the boundary-layer growth further, the temporal development of the displacement thickness δ^*, defined by

$$\delta^* = \int_0^\infty \left\{1 - \frac{u}{U_\infty}\right\} \mathrm{d}y, \tag{30}$$

is illustrated in figure 5. It may be observed that a substantial and accelerating thickening of the boundary layer is occurring in the region above the secondary eddy; furthermore, in the latter stages of the integrations, δ^* is approaching a vertical variation in the region near the right-hand side of the eddy.

It is evident from figures 4(*d*) and 5 that the boundary layer is entering a phase of rapidly strengthening boundary-layer growth. Furthermore, at the stages of the calculations illustrated in figure 4(*d*) it is apparent that the variations in the flow are so severe on the right-hand side of the eddy that the numerical mesh is inadequate there. At the same time it appears that at this point an interaction between the boundary layer and the outer flow is imminent. Consequently the calculations can only be carried on further in time (in the limit $Re \to \infty$) in the context of an appropriate rescaling of the Navier–Stokes equations which accounts for the possibility of an interaction; discussion of this aspect is deferred to §7.

Finally it is of interest to examine the development of the eddy. The stagnation

points defining the streamwise extent of the eddy spread outward as time increases; the positions of the stagnation points form sequences from which it is possible to estimate the limiting values. Doligalski (1980) has applied Shanks' (1955) (see also Van Dyke 1975, p. 203) transformation to the sequences, and estimates the large-time location of the stagnation points at $\xi = 1.667$ and at $\xi = 1.097$; note that these values should be regarded as no more than interesting extrapolations. Thus the rear stagnation point of the eddy successively appeared to approach the streamwise location of the rear stagnation point of the inviscid flow. To obtain another assessment of the limiting location of the eddy front stagnation point, the steady-state boundary-layer equations were numerically integrated in the ξ-direction from the inviscid front stagnation point at $\xi = 0.33$, where the solution is given by the Hiemenz (1911) stagnation-point solution, toward the rear stagnation point at $\xi = 1.667$ using a Crank–Nicolson-type integration scheme. These calculations showed that the wall shear stress vanished at $\xi = 1.06924$ which is reasonably close to the estimate of 1.097 obtained from the results of the unsteady calculations.

6. The convected vortex

As the fractional convection rate is increased from $\alpha = 0$ to progressively higher values, the development of the boundary layer gradually changes in character. This section is concerned with the effect of a convected vorticular disturbance on the boundary-layer development, and, to investigate the range $0 < \alpha < 1$ completely, results were obtained from $\alpha = 0.2$, 0.4, 0.55, 0.7, 0.75 and 0.80. It is worthwhile to emphasize that the majority of the streamline patterns presented here are relative to the vortex, and thus the vortex is towing the developing boundary-layer patterns with it as it moves along the plate.

The first case considered is $\alpha = 0.2$, for which the development of the boundary layer is illustrated in figures 6. Again, it may be observed from figure 6(*a*) at $t = 0.2$ that in the initial stages of the motion the flow patterns are almost symmetrical about the vortex centre. The streamline labelled -0.02 is a limiting streamline emanating from near the forward stagnation point and proceeding to upstream infinity; on the lower branch of this limiting streamline the direction of the flow is to the left from upstream infinity at $\xi = 0$ to downstream infinity at $\xi = 2$. Below the lower branch of the limiting streamline, all flow is to the left, and the arrows on the wall emphasize the fact that the wall is moving to the left in the convected coordinate system.

As time passes, the streamlines in the region near the wall and behind the vortex centre begin to lift up and develop a kink as illustrated in figure 6(*b*) at $t = 0.4$ in a manner similar to that observed for the stationary vortex. At $t_s = 0.424$ and at $\xi_s = 1.317$, $\eta_s = 0.297$ a boundary-layer separation occurs in the form of a closed recirculating eddy of positive rotation. This eddy occurs in the pocket forming between the lifting streamlines depicted in figure 6(*b*); the situation at $t = 0.6$ is illustrated in figure 6(*c*), where the separated eddy is fairly well developed and increasingly pushes up the limiting streamline labelled -0.02.

It is of interest to examine how the flow development would appear to an observer in the laboratory frame of reference. The streamlines in the laboratory frame are given by lines of constant Ψ_L, where

$$\Psi_L(\xi, \eta, t) = \Psi(\xi, \eta, t) + \beta\eta, \tag{31}$$

and Ψ is the stream function in the convected frame. In figure 6(*d*) the boundary-layer streamlines are plotted in the laboratory frame for the same case and time ($\alpha = 0.2$,

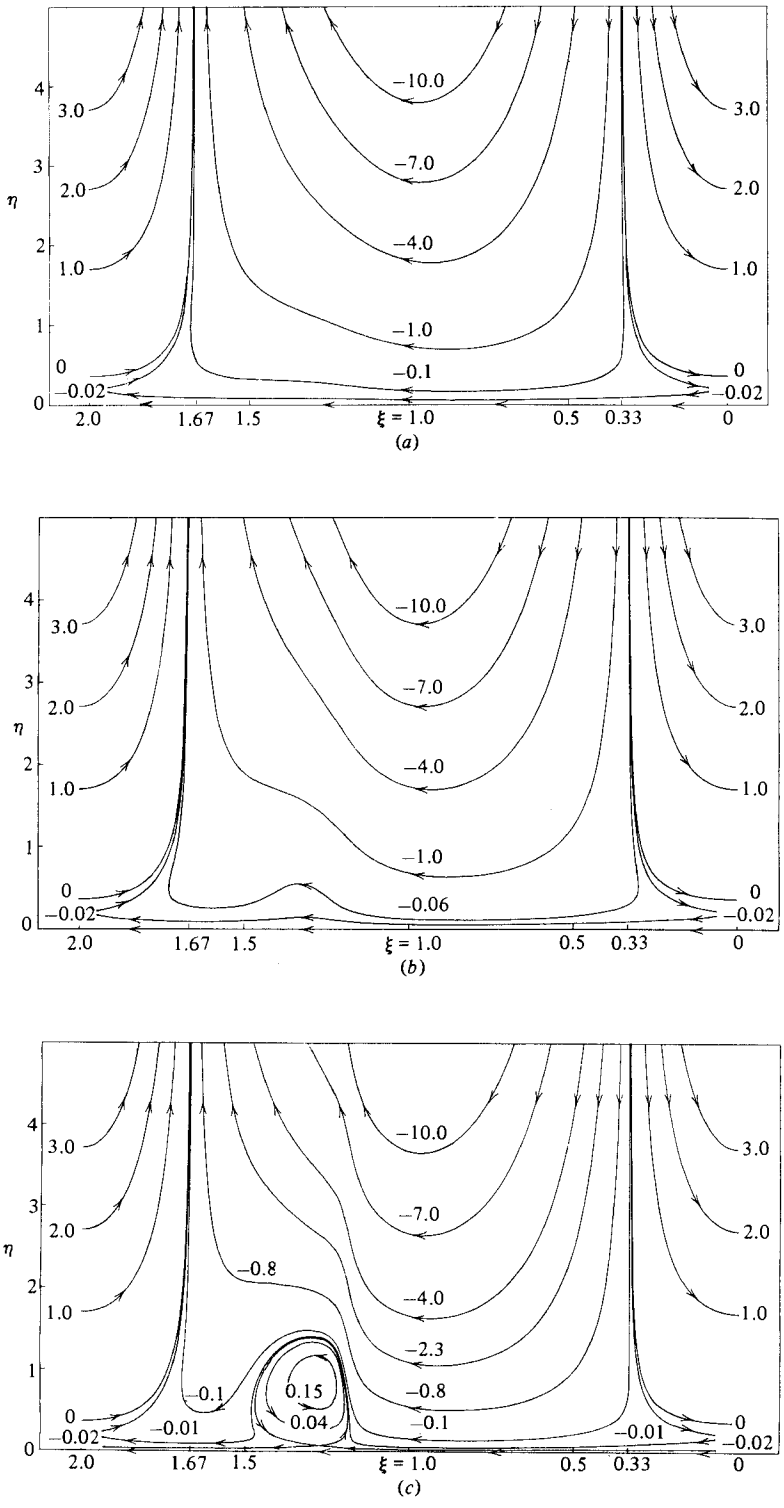

FIGURE 6(*a–c*). For caption see facing page.

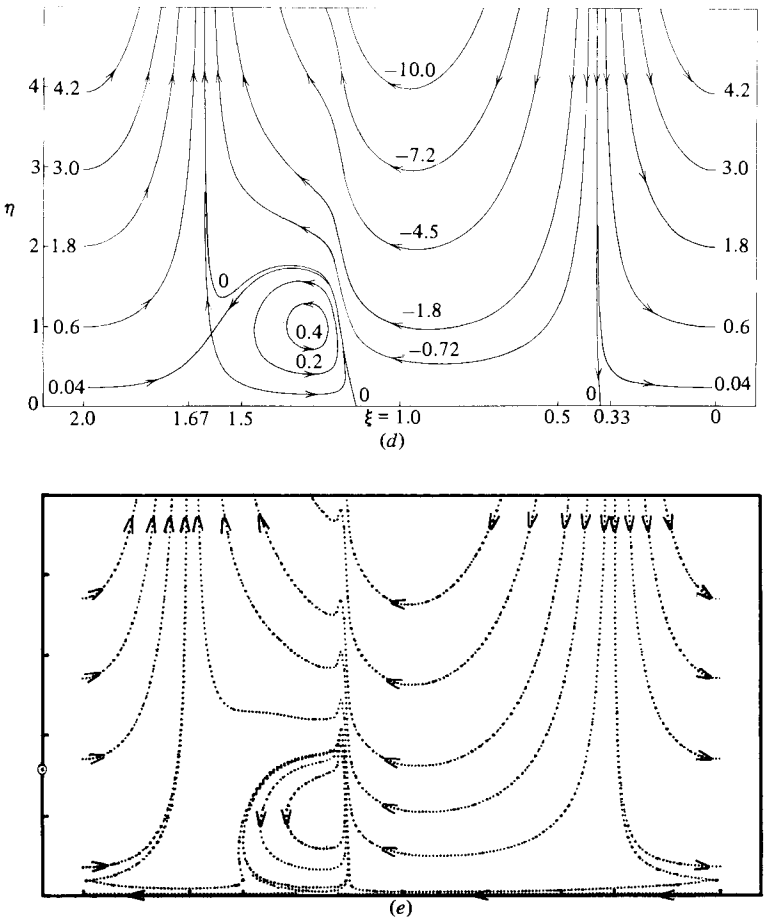

FIGURE 6. Instantaneous streamlines in the boundary layer for $\alpha = 0.2$: (*a*) relative to the vortex at $t = 0.2$, (*b*) relative to the vortex at $t = 0.4$, (*c*) relative to the vortex at $t = 0.6$, (*d*) relative to the laboratory frame at $t = 0.6$, (*e*) relative to the vortex at $t = 0.7$. (Labels correspond to lines of constant Ψ.)

$t = 0.6$) as the view in the convected frame in figure 6(*c*). It may be observed that a secondary recirculation eddy is also visible in the laboratory frame, but that it appears to be larger in extent and centred higher than when viewed in the convected frame. Note that apparent separation in the form of a detached eddy occurs first in the laboratory frame and is quickly followed by a separation in the convected reference frame.

Just as in the case of the stationary vortex, intense variations begin to develop in the flow field once the streamwise growth of the eddy is almost complete. This behaviour occurs along the right-hand side of the eddy and ultimately leads to the onset of a spike-like behaviour in the streamlines; this is illustrated in figure 6(*e*) at $t = 0.7$. At this stage the numerical mesh is not small enough to cope adequately with the intense variations which have developed on the right-side of the eddy; shortly after $t = 0.7$ the alternate differencing scheme failed to converge and a further reduction in the mesh was not practical.

To illustrate the boundary-layer growth it is customary to compute the displacement thickness. However, in this case it is not possible to define a conventional

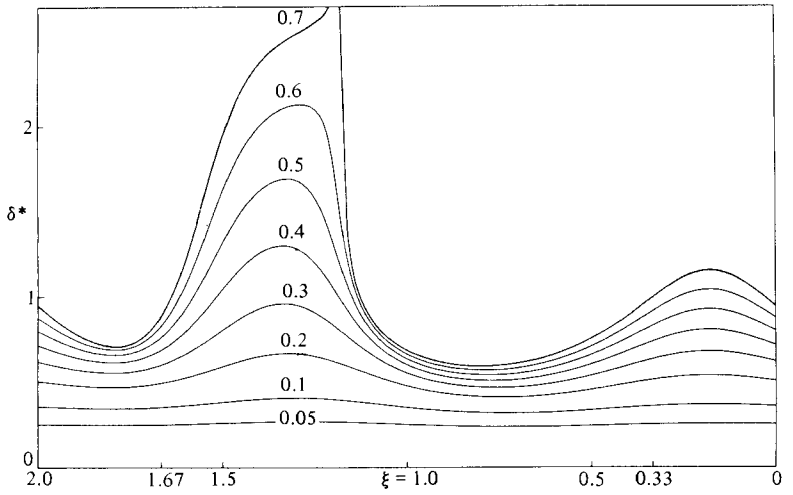

FIGURE 7. Temporal development of displacement thickness parameters for $\alpha = 0.2$. (Labels correspond to values of t.)

displacement thickness which has meaning for all ξ; this is because the inviscid flow has two stagnation points on the wall in the range $0 \leqslant \alpha < 0.75$. As an alternative, it is possible to define a parameter similar to the displacement thickness using the normalized velocity defined by (20) according to

$$\delta_1^* = 2t^{\frac{1}{2}} \int_0^\infty (1 - U)\, \mathrm{d}\eta. \tag{32}$$

Note that for the stationary vortex ($\alpha = 0$) $\delta_1^* = \delta^*$. The temporal development of the thickness δ_1^* is illustrated in figure 7 for $\alpha = 0.2$; it may be observed that, in a manner similar to the stationary vortex, a substantial and accelerating thickening of the boundary layer occurs in the region above the spawned eddy. Again δ_1^* is approaching a vertical variation on the right-hand side of the eddy in the later stages of the integration. Note also that the region of accelerating boundary-layer growth is somewhat narrower in streamwise extent than for the stationary vortex in figure 5.

The next case considered is for $\alpha = 0.4$. The early development of the boundary-layer flow is similar to that for $\alpha = 0.2$, and the situation at $t = 0.6$ is illustrated in figure 8. The thickness δ_1^* is plotted in figure 9. It may be observed that a separation phenomenon similar to that for $\alpha = 0.2$ also occurs; the principal difference with the increased convection rate is that the streamwise extent of the separated eddy (and concomitant thickening of the boundary layer) has diminished. Moreover the region of expected interaction is being compressed toward the inviscid rear stagnation point. This trend continues as illustrated in figure 10, where the flow-pattern development for $\alpha = 0.55$ is given. The lifting streamlines in figure 10 (a) ultimately yield to a rather small separated eddy in figure 10 (b) at $t = 0.7$. In figure 10 (c) the streamline pattern in the laboratory frame is illustrated at the same time as the convected view in figure 10 (b); an eddy is also observed in the laboratory frame but at a different location. Finally the numerical method fails and an indication of the reason is given in figure 10 (d), where the streamlines at $t = 0.8$ are plotted; this stage corresponds to a time shortly before failure of the calculations.

In figure 11 the streamline patterns for $\alpha = 0.7$ are plotted in a later stage of the calculation. It is possible to carry this computation somewhat further in time, but

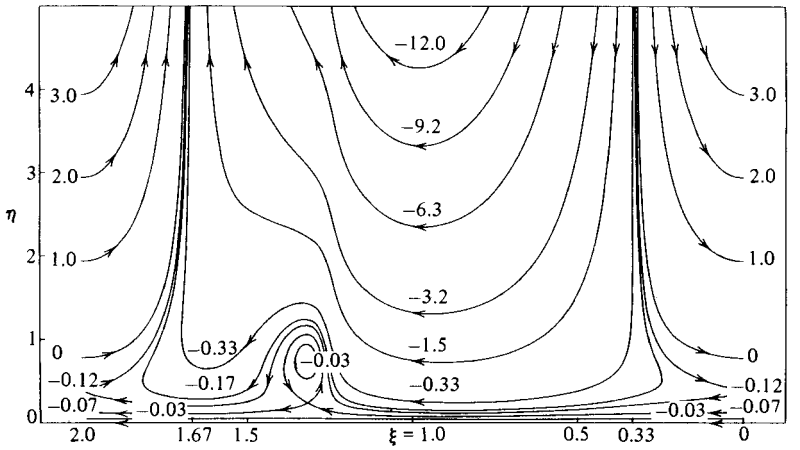

FIGURE 8. Instantaneous streamlines in the boundary layer for $\alpha = 0.4$ at $t = 0.6$ relative to the vortex. (Labels correspond to lines of constant Ψ.)

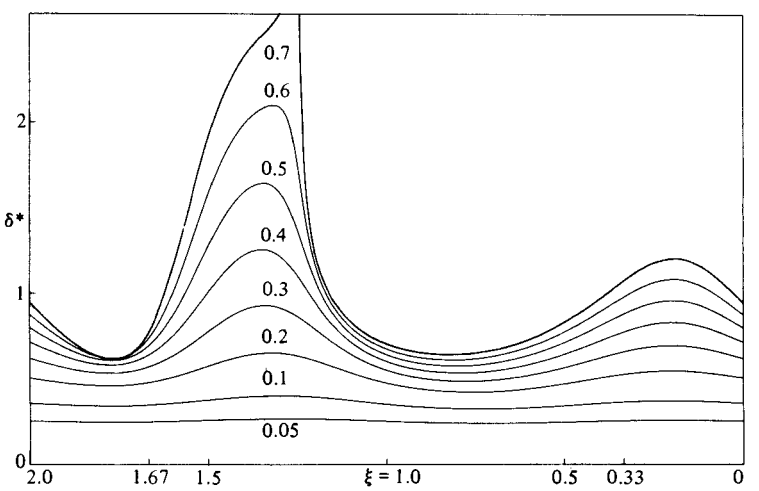

FIGURE 9. Temporal development of the displacement thickness parameter for $\alpha = 0.4$. (Labels correspond to values of t.)

again failure ultimately occurs. In this case no separation was observed to occur (at least until the calculations had to be stopped) but a pronounced kinking of the streamlines does take place near the rear stagnation point. Substantial boundary-layer growth occurs in the region near the stagnation point, but now in a very narrow band in the streamwise direction.

For $\alpha \geqslant 0.75$ an important change occurs in the boundary-layer flow. In these cases no kinking of the streamlines occurs and the integrations may be continued for somewhat longer times. The streamlines for $\alpha = 0.75$ and $\alpha = 0.8$ are plotted in both the convected frame and the laboratory frame in figures 12 and 13. By moving the outer boundary to progressively larger values the integrations could be continued longer than for the cases of $\alpha < 0.75$, but ultimately substantial boundary-layer growth also occurs. This growth is not readily apparent from the streamline patterns illustrated in figures 12 and 13, and, to illustrate this feature, a conventional

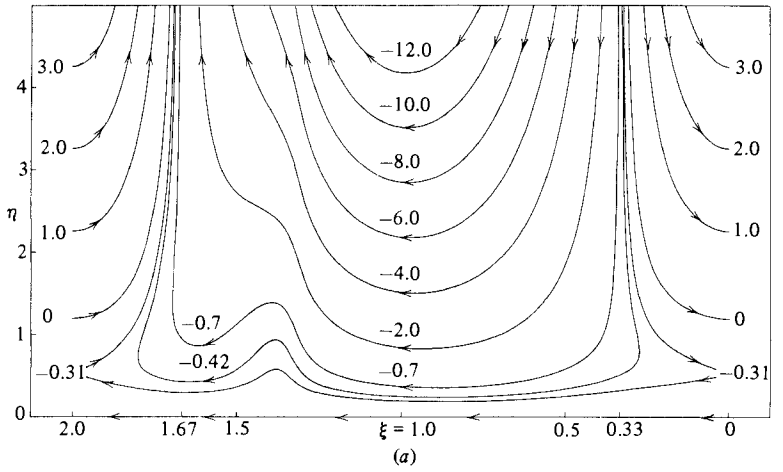

(a)

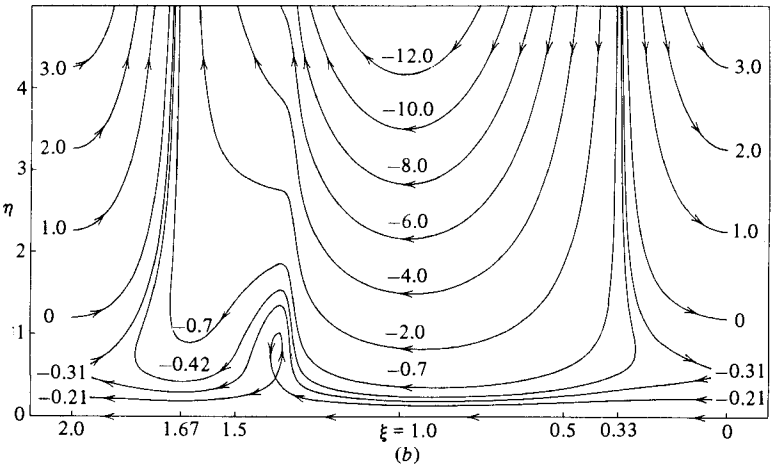

(b)

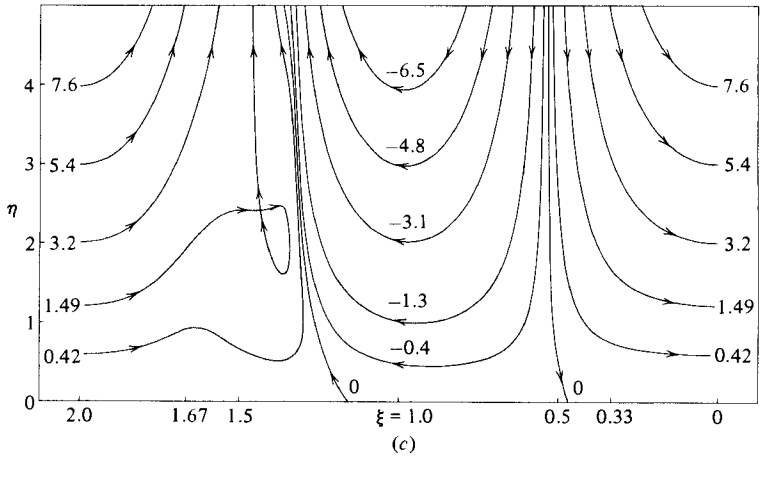

(c)

FIGURE 10(a–c). For caption see facing page.

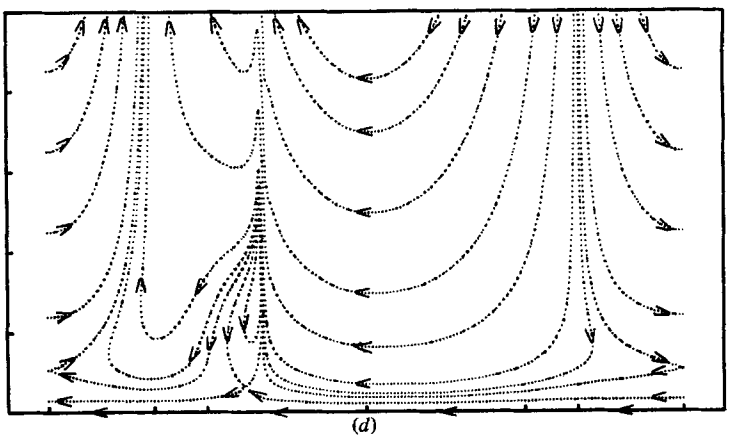

FIGURE 10. Instantaneous streamlines in the boundary layer for $\alpha = 0.55$: (*a*) relative to the vortex at $t = 0.6$, (*b*) relative to the vortex at $t = 0.7$, (*c*) relative to the laboratory frame at $t = 0.7$, (*d*) relative to the vortex at $t = 0.8$. (Labels correspond to lines of constant Ψ.)

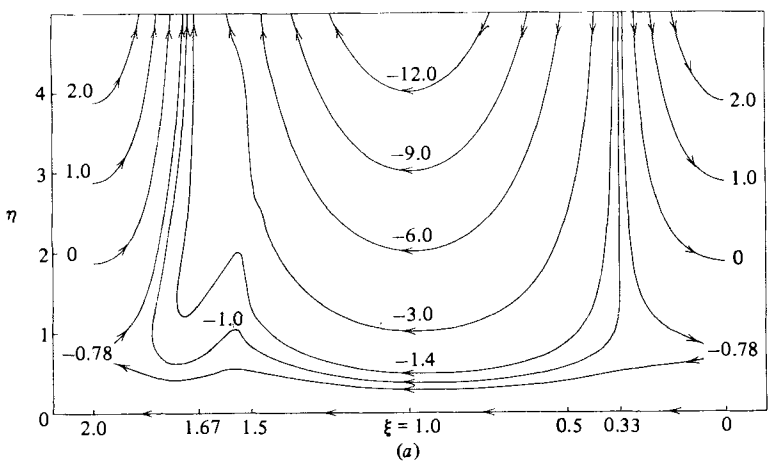

FIGURE 11. Instantaneous streamlines in the boundary layer for $\alpha = 0.7$ at $t = 1.0$: (*a*) relative to the vortex; (*b*) relative to the laboratory frame. (Labels correspond to values of constant Ψ.)

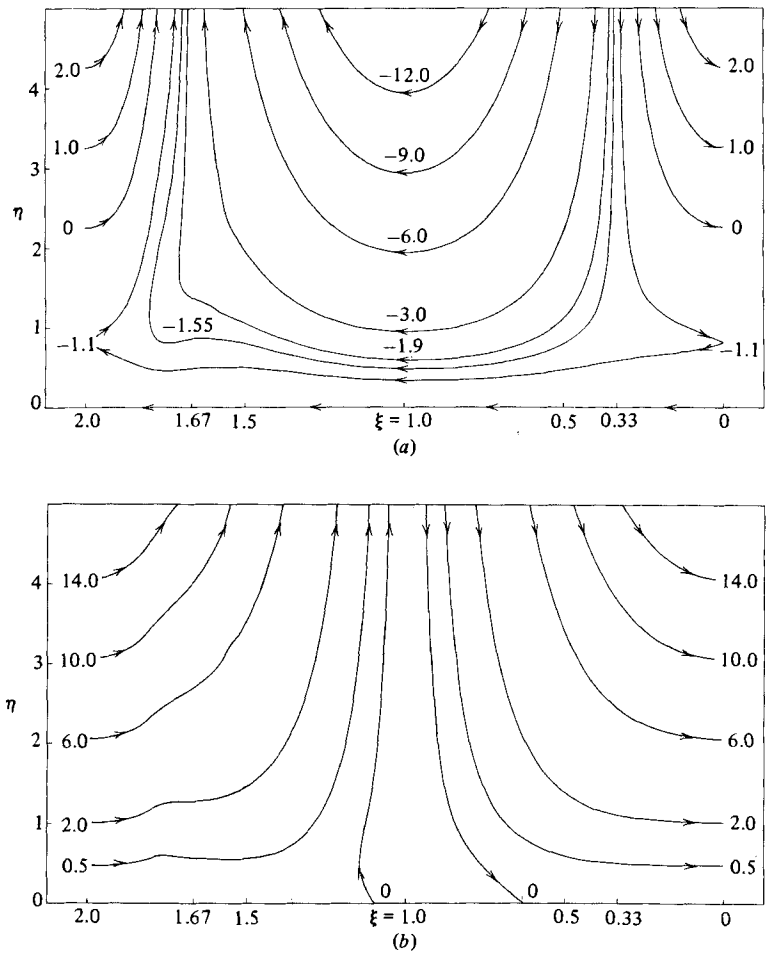

FIGURE 12. Instantaneous streamlines in the boundary layer for $\alpha = 0.75$ at $t = 1.0$: (*a*) relative to the vortex, (*b*) relative to the laboratory frame. (Labels correspond to lines of constant Ψ.)

displacement thickness is defined with respect to the velocity in the laboratory frame according to

$$\delta^* = \int_0^\infty \left\{1 + \frac{U+\beta}{2\cos\pi\xi - 1 + \beta}\right\} \mathrm{d}\eta. \tag{33}$$

The temporal development of δ^* is plotted in figure 14 for $\alpha = 0.8$, where the accelerated boundary-layer growth near the rear stagnation point should be noted. The displacement effect illustrated in figure 14 corresponds to the effect that an observer in the laboratory frame would see at fixed values of time. Note that in the laboratory frame the effect could be interpreted as a moving wave of growing amplitude.

Finally it is worthwhile to emphasize that, while it has been convenient to present the flow patterns in the (ξ, η)-plane, some distortion occurs in the streamwise direction. In figure 15 the streamline patterns in the convected frame for $\alpha = 0.8$ are plotted for the time illustrated in figure 13(*a*) in the physical (x, η)-plane. Comparison of figures 13(*a*) and 15 is useful to gain an appreciation of the distortion in the ξ-coordinate; basically the region between the inviscid stagnation points is magnified while the regions at upstream and downstream infinity are compressed.

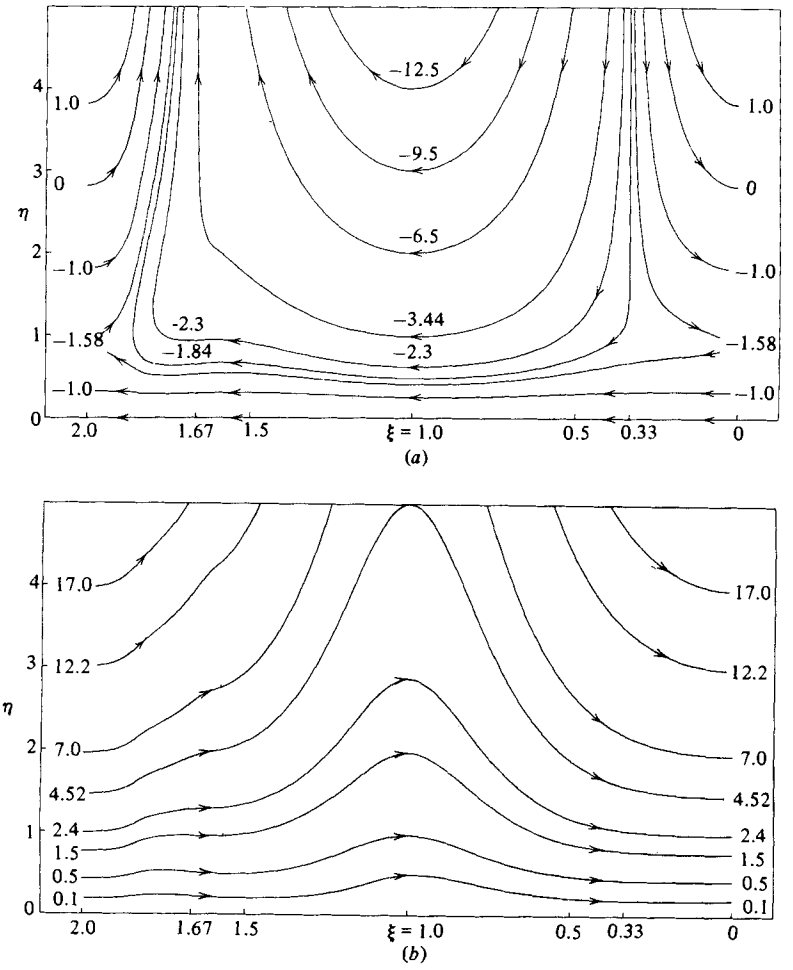

FIGURE 13. Instantaneous streamlines in the boundary layer for $\alpha = 0.8$ at $t = 1.1$: (*a*) relative to the vortex, (*b*) relative to the laboratory frame. (Labels correspond to lines of constant Ψ.)

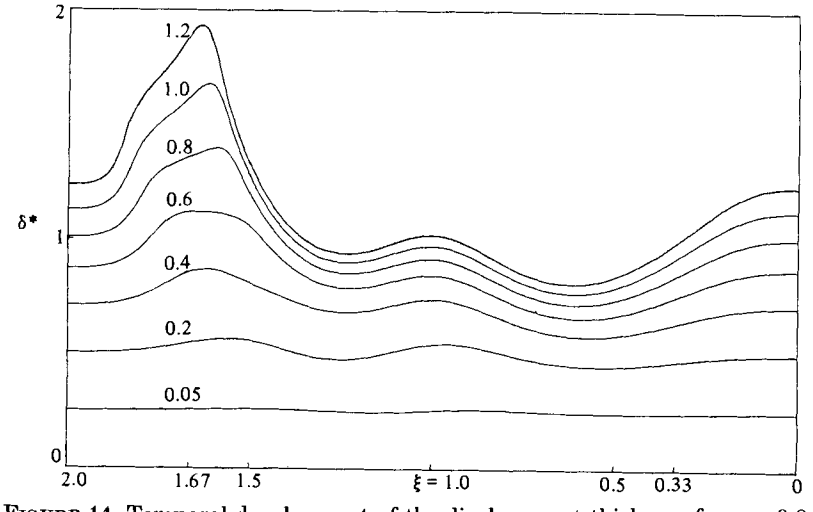

FIGURE 14. Temporal development of the displacement thickness for $\alpha = 0.8$. (Labels correspond to values of t.)

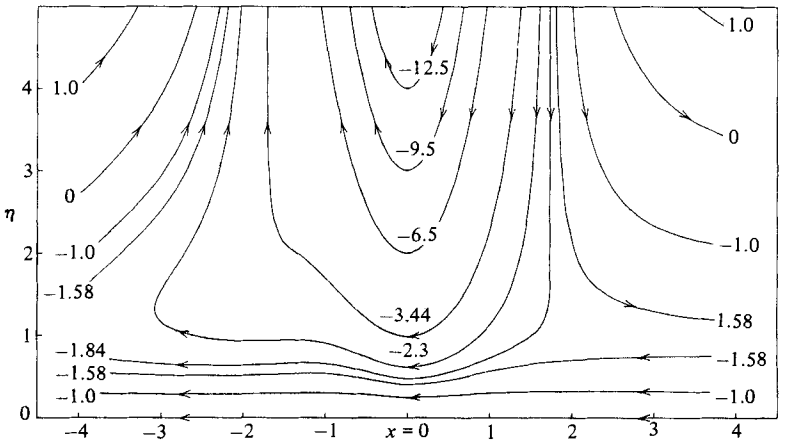

FIGURE 15. Instantaneous streamlines in the boundary layer relative to the vortex in the physical streamwise scale for $\alpha = 0.8$ at $t = 1.1$. (Labels correspond to lines of constant Ψ.)

7. Discussion of results

In view of the calculated results of §6, it is reasonable to conclude that the unsteady boundary layer induced by a convected vortex in a uniform flow will eventually interact strongly with the outer inviscid flow for any convection speed. The boundary-layer development depends on the value of the fractional convection rate α and a rate of $\alpha = 0.75$ corresponds to a critical situation. For convection rates such that $\alpha < 0.75$, a lifting and subsequent kinking of the streamlines always occurs in the region behind the vortex. For values of $\alpha \leqslant 0.55$, a separation phenomenon in the form of a separated detached eddy was observed to initiate near the wall in the pocket formed by the kinking streamlines. Once separation occurs the eddy grows rapidly in the direction normal to the wall and very intense variations begin to develop on the right-hand side of the eddy. In the latter stages of the integrations, a spike-like behaviour begins to develop in the streamlines, and the calculations cannot be continued; evidently the flow is close to an inviscid–viscous interaction at this point. The eddy that is created in the boundary layer is in all cases of positive rotation (which is opposite to the parent vortex in the inviscid flow). As α increases, the relative width of the boundary-layer eddy diminishes and the region of strong boundary-layer growth narrows toward the rear stagnation point. Finally for $\alpha = 0.7$ no separated zone was observed, although severe kinking of the streamlines in a very narrow region near $\xi = 1.67$ occurred. In all cases, where separation and/or streamline liftup and kinking occurs, an abrupt and rapid thickening of the boundary layer takes place. On the other hand, for $\alpha \geqslant 0.75$, the development of the boundary-layer flow is somewhat more gradual, and the integrations could be carried on to relatively larger times; however, again substantial boundary-layer growth ultimately occurs in the region behind the vortex.

The principal difference between the two regimes can be understood as follows. The boundary-layer flow in the convected reference frame is subject to two influences, namely the inviscid flow near the wall and the effect of wall moving to the left. With reference to the dimensionless variables in (6)–(9), it may be confirmed that the maximum velocity is -3 at $\xi = 1$ immediately below the vortex centre; the velocity of the wall to the left is $-\beta$. For $\alpha < 0.75$, $\beta < 3$ and the maximum velocity in the inviscid flow is greater than the wall speed. Consequently in such cases the inviscid

flow exerts a dominant effect, and the relative streamlines in the boundary layer are lifted behind the vortex even near the wall; this process may be thought of as a reaming action by the vortex on the boundary layer. Note, however, that, as the rear stagnation point is approached from the right, the magnitude of the inviscid velocity decreases and the moving wall begins to exert the dominant effect; it may be observed for example in figure 10(*b*) that the boundary-layer fluid near the wall and near $\xi = 1.67$ is not lifted but is dragged to the left. Thus for $\alpha < 0.75$ a kink develops in the lifted streamlines, and subsequently a separated eddy occurs in the flow in most cases. On the other hand, for $\alpha > 0.75$, $\beta > 3$ and the wall moves to the left at a greater rate than any speed in the inviscid flow. In these cases, the left-moving wall exerts the dominant effect near the wall and no kinking of the streamlines occurs. However, the flow in the outer part of the boundary layer is exposed to an outflow stagnation-point flow at $\xi = 1.67$, and this ultimately leads to substantial boundary-layer growth but now in a very narrow band in the streamwise direction.

For all cases considered, the results suggest that the local thickening of the boundary layer will continue to accelerate, and once the thickness of the layer becomes comparable to the lengthscale of the outer flow, breakdown of the classical thin boundary-layer picture will occur in the form of an inviscid–viscous interaction. The precise nature of the interaction is not known, and further progress is impeded by ignorance of the terminal form (immediately before breakdown) of the boundary-layer solution. However, the calculated results are suggestive of the early stages of the formation of a singular behaviour at finite time and appear to be qualitatively similar to some of the notions behind the Moore–Rott–Sears model of unsteady separation. This model was originally proposed by Sears & Telionis (1975) as a general model of unsteady separation; in the MRS model the separation point is defined as that location where the velocity and shear stress vanish in a singular manner as seen by an observer moving with the separation. Note that this definition implies the classical idea of breakdown, since, once a singularity begins to evolve in the boundary-layer solution, changes in the outer inviscid flow must begin to take place. A number of attempts have been made to substantiate the MRS model (Sears & Telionis 1975; Williams 1977) by computation of various unsteady boundary-layer flows, particularly the impulsively started circular cylinder (Belcher *et al.* 1971; Collins & Dennis 1973, Cebeci 1979, Ece, Walker & Doligalski 1983). Until recently the implications of these numerical studies have been controversial because of difficulties similar to those encountered here; once detached eddies occur in the boundary-layer flow, intense variations in the velocity field begin to develop near the eddy and it becomes increasingly difficult to maintain good accuracy in the numerical solution; consequently whether or not an MRS condition and a singular behaviour develop at finite time has been a matter of some debate. Recently, the first rational account of the terminal nature of the boundary-layer flow for an impulsively started cylinder has been given by Van Dommelen (1981) and Van Dommelen & Shen (1980), who also calculate a numerical solution but in Lagrangian coordinates (see also Elliot, Cowley & Smith 1983). These studies support the MRS condition as the appropriate condition for boundary-layer breakdown and demonstrate that a singularity does occur in the boundary-layer solution at finite time.

In the present numerical results, the boundary-layer solution does appear to be evolving toward an MRS condition, at least for $\alpha < 0.75$. It may be observed in figures 4(*c*), 6(*c*), 8, 10(*b*) and 11 that the streamlines in the boundary layer near the upstream side of the detached eddies are ultimately deflected in a direction which is almost normal to the wall; the flow patterns near these eddies are of the type

sketched by Van Dommelen (1981) (figure 21, p. 237) for the expected streamlines near an MRS point corresponding to a downstream-moving wall. Although the numerical results are suggestive that an MRS condition will ultimately occur, there is at present no confirming analytical evidence for a singularity at finite time in the present study. On the other hand, the indication that the flows for all α are approaching an interactive phase is strong; unfortunately the methods required to treat strong inviscid–viscous interactions are not known and for the present it is only possible to speculate on the nature of the expected interaction. At the lower convection rates, it appears likely that the eddy spawned in the boundary layer will be ejected in a manner similar to that observed by Harvey & Perry (1971). As α increases beyond 0.75, the integrations suggest the boundary layer may erupt in a jet-like manner. This conjecture is supported by the experiments of Doligalski *et al.* (1980) for a vortex with $\alpha = 0.9$ convecting over an established flat-plate boundary layer; in these experiments the erupting fluid subsequently appeared to be rolled over into another vortex.

In this study an impulsive-start initial condition was used and a question that arises is whether or not the impulsive start could be the cause of the breakdown. Such an initial condition cannot be exactly duplicated in the laboratory and was chosen here as a convenient initial state that involves no initial disturbance to the inviscid flow. Other initial conditions may be considered corresponding, for example, to a gradual imposition of the mainstream velocity; in such cases the initial flow in the boundary layer is again almost symmetrical (see e.g. figure 4*a*). The point is that the intense variations and detached eddies that occur in the present calculations appear only after the boundary layer is exposed to the action of the vortex for a period of time. Thus it is the effect of the vortex that is believed to drive the boundary-layer flow toward interaction rather than the particular initial flow.

It is of interest to briefly examine the possible relevance of the present study to bursting in fully developed turbulent boundary layers. The mean-velocity profile in the outer layer of a nominally steady two-dimensional turbulent boundary layer is a uniform flow to leading order (Fendell 1972) combined with a lower-order shear flow; consequently at locations remote from the wall the composite mean profile is a weakly sheared uniform flow. Convected discrete vorticular motions are observed to be an important feature of the outer-layer flow (Falco 1977, 1978, 1982; Head & Bandyopadhyay 1981). The apparently active vortices near the wall are believed to have a typical lengthscale of the order of 100 wall-layer units; these convected vortices are three-dimensional and are more complex than the two-dimensional filaments discussed in this paper. Indeed all real vortices are three-dimensional (Lighthill 1963) and a two-dimensional vortex can only be viewed as a mathematical idealization of a portion of three-dimensinal filament. It has previously been suggested by various authors (Nychas *et al.* 1973; Doligalski *et al.* 1981) that vortex motions can play a role in triggering the observed eruptions of fluid from the wall-layer region. The results of the present study suggest how this might occur. When a convected vortex is strong enough and/or close enough to the wall, an unsteady viscous effect is induced in the viscous region near the wall; as the vortex convects downstream it carries a separating region with it. Ultimately the effect builds in intensity and an eruption into the outer layer occurs. This conjectured type of cyclical process offers a possible explanation of how new vorticity is continually introduced into the outer layer. However, the phenomena and vortex motions in a turbulent flow are more complex than the physical situations considered in this paper; for this reason the physical mechanism for regeneration proposed here requires further study.

Finally, the calculations in the present study have been carried out for a rectilinear filament, and it is of interest to inquire whether the present results have wider applicability to vortex motions in two dimensions. The rectilinear vortex represents one limit of vortex motion in which the vorticity is highly concentrated in a small core region. Batchelor (1967, p. 534) has described the other possible limit of two-dimensional vortex motion in which the vorticity is distributed over a finite area in the inviscid region. If (r, θ) are polar coordinates measured from an origin on an infinite plane wall, a stream function ψ can be defined in the usual way and a solution of the inviscid equations that has zero vorticity for $r > e$ and vorticity proportional to ψ for $r < e$ is

$$\left.\begin{aligned} \psi &= \left\{r - \frac{e^2}{r}\right\} \sin\theta \quad (r > e), \\ &= 2U_\infty \frac{J_1(jr)}{jJ_0(je)} \sin\theta \quad (r \leqslant e). \end{aligned}\right\} \tag{34}$$

Here J_0 and J_1 are Bessel functions and $j = \lambda_i/e$, where λ_i is the ith zero of J_1. This solution represents a vortex embedded in a uniform flow having speed U_∞ at infinity with vorticity spread over the half-circle $r = e$. If the wall is now imagined to move to the left, then an observer on the wall would see a vortex of negative rotation moving to the right. A variety of solutions are possible corresponding to the particular value of λ_i chosen. Consider the first zero given by $\lambda_i = 3.8317$; it may easily be verified that the single-celled vortex corresponding to this case produces a streamline pattern very similar to that illustrated in figure 1 (*d*) for the rectilinear filament. The vortex centre is at $r_0 = 0.48e$, and the stagnation points occur on the wall at $x = \pm 2.09r_0$ as opposed to $\pm 1.73a$ for the rectilinear filament. Rather than $\alpha = 0.75$, the critical value for this vortex may be shown to be $\alpha = 0.713$. Because of the close similarity in the inviscid flows, the boundary layer is expected to respond in a very similar manner for this type of vortex. Lastly it is of some interest to note that vortices having cells of alternating rotation may be obtained by taking high-order zeros λ_i in (34); such vortices have multiple outflow stagnation points near the wall and presumably would be able to induce multiple boundary-layer eruptions.

The authors are grateful for support of this study by the Air Force Office of Scientific Research under contract no. F49620-78-C-0071.

REFERENCES

BATCHELOR, G. K. 1967 *An Introduction to Fluid Dynamics*. Cambridge University Press.

BELCHER, R. J., BURGGRAF, O. R., COOKE, J. C., ROBINS, A. J. & STEWARTSON, K. 1971 Limit-less boundary layers. In *Recent Research on Unsteady Boundary Layers*, pp. 1444–1446. Laval University Press. Quebec, Canada.

BLASIUS, H. 1908 Grenzschichten in Flüssigkeiten mit kleiner Reibung. *Z. Math. Phys.* **56**, 1–37.

CEBECI, T. 1979 The laminar boundary layer on a circular cylinder started impulsively from rest. *J. Comp. Phys.* **31**, 153–172.

CLEMENTS, R. R. & MAULL, D. J. 1975 The representation of sheets of vorticity by discrete vortices. *Prog. Aero. Sci.* **16**, 129–146.

COLLINS, W. M. & DENNIS, S. C. R. .1973 Flow past an impulsively started circular cylinder. *J. Fluid Mech.* **60**, 105–127.

DENNIS, S. C. R. & WALKER, J. D. A. 1971 The initial flow past an impulsively started sphere at high Reynolds numbers. *J. Engng Maths* **5**, 263–278.

DENNIS, S. C. R. & WALKER, J. D. A. 1972 Numerical solutions for time-dependent flow past an impulsively started sphere. *Phys. Fluids* **15**, 517–525.

DOLIGALSKI, T. L. 1980 The influence of vortex motion on wall boundary layers. Ph.D. dissertation, Lehigh University.

DOLIGALSKI, T. L., SMITH, C. R. & WALKER, J. D. A. 1980 A production mechanism for turbulent boundary layers. In *Viscous Drag Reduction* (ed. G. Hough); *Prog. Astro. Aero.* **72**, 47–72.

ELLIOT, J. W., COWLEY, S. J. & SMITH, F. T. 1983 Breakdown of boundary layers. *Geophys. Astrophys. Fluid Dyn.* (to appear).

ECE, M. C., WALKER, J. D. A. & DOLIGALSKI, T. L. 1983 The boundary layer on an impulsively started rotating and translating cylinder. *Phys. Fluids.* (to appear).

FALCO, R. E. 1977 Coherent motions in the outer region of turbulent boundary layers. *Phys. Fluids* Suppl. **20**, S124–S132.

FALCO, R. E. 1978 The role of outer flow coherent motions in the production of turbulence near a wall. In *Proc. AFOSR Workshop on Coherent Structure of Turbulent Boundary Layers* (ed. C. Smith & D. Abbott). Lehigh University.

FALCO, R. E. 1982 A synthesis and model of turbulence structure in the wall region. In *Structure of Turbulence in Heat and Mass Transfor* (ed. Z. P. Zaric). Hemisphere.

FENDELL, F. E. 1972 Singular perturbation and turbulent shear flow near walls. *J. Astro. Sci.* **20**, 129–165.

HARVEY, J. K. 1958 Some measurements on a yawed slender delta wing with leading edge separation. *British Aero. Res. Counc.* R&M 3160.

HARVEY, J. K. & PERRY, F. J. 1971 Flowfield produced by trailing vortices in the vicinity of the ground. *AIAA J.* **9**, 1659–1660.

HEAD, M. R. & BANDYOPADHYAY, P. 1981 New aspects of turbulent boundary-layer structure. *J. Fluid Mech.* **107**, 297–338.

HIEMENZ, K. 1911 Die Grenzschicht an einem in den gleichförmigen Flüssigkeitstrom eingetauchten geraden Kreiszylinder. *Dinglers J.* **326**, 321–323, 344–348, 357–362, 391–393, 409–410.

MACCORMACK, R. W. 1969 The effect of viscosity in hypervelocity impact cratering. *AIAA Paper* 69–354, Cincinnati, Ohio.

MILNE-THOMPSON, L. M. 1960 *Theoretical Hydrodynamics*, 4th edn. Macmillan.

NYCHAS, S. G., HERSHEY, H. C. & BRODKEY, R. S. 1973 A visual study of turbulent shear flow. *J. Fluid Mech.* **61**, 513–540.

ORNBERG, T. 1964 A note on the flow around delta wings. *Royal Inst. of Tech., Sweden, KTH-Aero* TN 38.

RAYLEIGH, LORD 1911 On the motion of solid bodies through viscous liquids. *Phil. Mag.* **21**, 697–711.

RILEY, N. 1975 Unsteady laminar boundary layers. *SIAM Rev.* **17**, 274–297.

SEARS, W. R. & TELIONIS, D. P. 1975 Boundary-layer separation in unsteady flow. *SIAM J. Appl. Maths* **28**, 215–235.

SHANKS, D. 1955 Nonlinear transformations of divergent and slowly convergent sequences. *J. Math. Phys.* **34**, 1–42.

VAN DOMMELEN, L. L. 1981 Unsteady boundary layer separation. Ph.D. thesis, Cornell University.

VAN DOMMELEN, L. L. & SHEN, S. F. 1980 The spontaneous generation of the singularity in a separating laminar boundary layer. *J. Comp. Phys.* **38**, 125–140.

VAN DYKE, M. 1975 *Perturbation Methods in Fluid Mechanics.* Parabolic.

WALKER, J. D. A. 1978 The boundary layer due to rectilinear vortex. *Proc. R. Soc. Lond.* A **359**, 167–188.

WILLMARTH, W. W. 1975 Structure of turbulence in boundary layers. *Adv. Appl. Mech.* **15**, 159–254.

WILLIAMS, J. C. 1977 Unsteady boundary layers. *Ann. Rev. Fluid. Mech.* **9**, 113–144.